AMERICAN ACADEMY™
OF OPHTHALMOLOGY

In Vivo 3-Dimensional Strain Mapping of the Optic Nerve Head Following Intraocular Pressure Lowering by Trabeculectomy

Michaël J.A. Girard, MSc, PhD,[1,2] *Meghna R. Beotra, BEng,*[1] *Khai Sing Chin, MSc,*[1] *Amanjeet Sandhu, FRCOphth,*[3] *Monica Clemo, BSc,*[3] *Eleni Nikita, FRCOphth,*[3] *Deborah S. Kamal, MD, FRCOphth,*[3] *Maria Papadopoulos, MBBS, FRACO,*[3] *Jean Martial Mari, PhD,*[4] *Tin Aung, FRCS, PhD,*[2] *Nicholas G. Strouthidis, MD, PhD*[2,3,5]

Purpose: To map the 3-dimensional (3D) strain of the optic nerve head (ONH) in vivo after intraocular pressure (IOP) lowering by trabeculectomy (TE) and to establish associations between ONH strain and retinal sensitivity.

Design: Observational case series.

Participants: Nine patients with primary open-angle glaucoma (POAG) and 3 normal controls.

Methods: The ONHs of 9 subjects with POAG (pre-TE IOP: 25.3±13.9 mmHg; post-TE IOP: 11.8±8.6 mmHg) were imaged (1 eye per subject) using optical coherence tomography (OCT) (Heidelberg Spectralis, Heidelberg Engineering GmbH, Heidelberg, Germany) before (<21 days) and after (<50 days) TE. The imaging protocol was repeated for 3 controls in whom IOP was not altered. In each post-TE OCT volume, 4 tissues were manually segmented (prelamina, choroid, sclera, and lamina cribrosa [LC]). For each ONH, a 3D tracking algorithm was applied to both post- and pre-TE OCT volumes to extract IOP-induced 3D displacements at segmented nodes. Displacements were filtered, smoothed, and processed to extract 3D strain relief (the amount of tissue deformation relieved after TE). Strain relief was compared with measures of retinal sensitivity from visual field testing.

Main Outcome Measures: Three-dimensional ONH displacements and strain relief.

Results: On average, strain relief (averaged or effective component) in the glaucoma ONHs (8.6%) due to TE was higher than that measured in the normal controls (1.07%). We found no associations between the magnitude of IOP decrease and the LC strain relief ($P > 0.05$), suggesting biomechanical variability across subjects. The LC displaced posteriorly, anteriorly, or not at all. Furthermore, we found linear associations between retinal sensitivity and LC effective strain relief ($P < 0.001$; high strain relief associated with low retinal sensitivity).

Conclusions: We demonstrate that ONH displacements and strains can be measured in vivo and that TE can relieve ONH strains. Our data suggest a wide variability in ONH biomechanics in the subjects examined in this study. We further demonstrate associations between LC effective strain relief and retinal sensitivity. *Ophthalmology 2016;■:1–11 © 2016 by the American Academy of Ophthalmology.*

Supplemental material is available at www.aaojournal.org.

Elevated intraocular pressure (IOP) is associated with increased prevalence[1] and incidence[2] of glaucoma. However, some patients with elevated IOP never develop glaucoma. Furthermore, glaucoma occurs nearly as often in patients with normal levels of IOP as in those with elevated levels[3] and does so without a distinctly different etiology.[4] In brief, our current understanding of glaucoma is insufficient: We know that IOP is an important, albeit not the only, predisposing risk factor in the development and progression of this pathology.[2]

Our previous research[5,6] and that of other investigators[7,8] have set out to provide explanations for these clinical observations and suggested that the biomechanics of an individual's optic nerve head (ONH) dictate the IOP level it can sustain without inducing glaucomatous damage. Above an individual specific threshold level of IOP, a series of cellular events could be initiated at the level of the lamina cribrosa (LC)—a putative major site of damage in glaucoma—and eventually lead to glaucomatous damage. Unfortunately, no studies have been able to test such biomechanical hypotheses directly because most were limited to postmortem experiments[5,9–12] or computational modeling.[13–16] We believe that if it were possible to directly characterize ONH biomechanics in the living human eye, this may represent an accurate predictor for future glaucoma progression.[17]

Several studies have claimed measurements of IOP-induced ONH "deformations" in vivo using optical coherence tomography (OCT), especially at the site of the LC. Agoumi et al[18] were the first to use OCT to investigate LC displacements in patients with glaucoma after changes in IOP through ophthalmodynamometry, but they found

http://dx.doi.org/10.1016/j.ophtha.2016.02.008
ISSN 0161-6420/16

inconclusive evidence for LC movements after an acute IOP elevation of approximately 12 mmHg.[18] Further studies in both monkeys and humans reported changes in anterior LC surface configurations (LC depth) with IOP increases[19] or IOP lowering after trabeculectomy (TE).[20–25] However, LC depth is a poor surrogate for LC deformations, and none of the aforementioned studies have been able to map in vivo IOP-induced 3-dimensional (3D) displacements and strains (the engineering definition for deformation) that could indicate local compression, shear, or stretch of the axons passing through the LC. Such information is of critical value if we want to understand how local ONH deformations could lead to RGC damage and apoptosis. All prior studies also have been hampered by restricted LC visibility in OCT.[26,27]

The aim of this study was to establish a foundation for mapping ONH biomechanical characteristics in patients. In our previous work, we proposed and verified (but not validated) an OCT-based 3D tracking algorithm that could extract IOP-induced ONH displacements and strains after a change in IOP.[28] By using this novel technique, we report here in vivo local displacement/strain mapping of ONH tissues after IOP lowering by TE in subjects with glaucoma and establish associations with visual field loss.

Methods

Patient Recruitment and Trabeculectomy

This study was approved by the Bloomsbury Research Ethics Committee, United Kingdom, and adhered to the ethical principles outlined in the Declaration of Helsinki. All recruited subjects gave written informed consent. Inclusion criteria for healthy controls ($n = 3$) were IOP $\leq$21 mm Hg, healthy ONHs with vertical cup-to-disc ratio $\leq$0.5, and normal visual fields. These subjects were not attending the hospital eye service for any clinical reason and had no other relevant pathology. In addition, 9 subjects with primary open-angle glaucoma (POAG) who were to undergo TE as part of their standard clinical care were recruited.

Primary open-angle glaucoma was defined as glaucomatous optic neuropathy, characterized as loss of neuroretinal rim with vertical cup-to-disc ratio >0.7 or focal notching with nerve fiber layer defect attributable to glaucoma and/or asymmetry of cup-to-disc ratio between eyes >0.2, with repeatable glaucomatous visual field defects (independent of the IOP value) in at least 1 eye.

The decision to perform TE was not made on the basis of participation in the study but after detection of visual field progression despite the use of 3 or more topical IOP-lowering agents as per UK National Institute of Clinical Excellence guidance.[29] All surgery was undertaken by 1 of 3 glaucoma fellowship–trained consultant surgeons (D.S.K., M.P., N.G.S.). The surgical method in all cases adhered to the technique described as the Moorfields Safer Surgery Technique.[30] In all cases, mitomycin C 0.2 mg/ml was used. Postoperative management involved a gradual reduction of IOP through adjustment and removal of sutures in the first 4 weeks after the surgery. One subject with POAG was excluded from analysis, because IOP lowering was not achieved by the time of postoperative imaging. Demographics and clinical data for all included subjects are listed in Table 1.

Optical Coherence Tomography Imaging

After pupillary dilatation (1% tropicamide), each glaucoma subject's ONH was imaged twice using enhanced-depth imaging spectral-domain OCT (Spectralis, Heidelberg Engineering GmbH, Heidelberg, Germany). The first acquisition was performed before TE (within 21 days) when IOP was medically treated but inadequately controlled. The second acquisition was performed after TE when target IOP had been achieved without medication (within 50 days) (Table 1). Each OCT volume (horizontal raster) comprised 145 horizontal B-scans (each composed of 384 A-scans) covering a rectangular region of 15°×15° centered on the ONH. The average distance between 2 consecutive B-scans was 30.59 μm, and the axial and lateral B-scan pixel resolutions were 3.87 μm and 11.49 μm, respectively. Note that all A-scans were averaged 10 times during acquisition to reduce speckle noise. The OCT imaging protocol was repeated for the 3 normal controls except that both OCT volumes were acquired consecutively at the same visit with no IOP manipulation.

Visual Field Testing

All subjects with POAG underwent static automated perimetry using the Humphrey Field Analyzer (Carl Zeiss Meditec, Dublin, CA), 24-2 SITA Standard test protocol. Each subject was an experienced visual field witness (>7 previous tests), and all tests included in this study were reliable (<20% fixation losses, <33% false-positives, <33% false-negatives). All visual fields were undertaken within 12 weeks before TE surgery and processed to extract "raw" retinal sensitivity values (in decibels).

Light Attenuation Correction Using Adaptive Compensation

To remove light-attenuation artefacts, all OCT volumes were postprocessed using adaptive compensation (AC).[27,31] In OCT images, AC has been shown to improve tissue visibility below blood vessel shadows and to improve the visibility/contrast of the LC/choroid/scleral boundaries and of the LC insertions into the sclera.[26,32] In addition, our previous work has indicated that AC can improve the accuracy of 3D displacement tracking when 10× signal averaging was used[28] (as performed in this article).

Optic Nerve Head Reconstruction through Manual Segmentation

In this study, we aim to establish the characteristic deformation pattern of each major ONH tissue after a change in IOP. To this end, each compensated post-TE (lower-IOP) OCT volume was manually segmented (i.e., digitally partitioned) using Amira (version 5.4, FEI, Hillsboro, OR) to identify the following tissue groups: (1) choroid, Bruch's membrane, and retinal pigment epithelium; (2) peripapillary sclera; (3) LC; and (4) prelaminar tissues (Fig 1). Note that all segmentations were cropped (Fig 1) to ensure that only overlapping ONH image regions (pre- and post-TE) were used for 3D tracking. Note also that segmentations were conducted only when tissue was visible as detected from the compensated OCT signal. In most cases, full-thickness segmentation of the LC and sclera could not be achieved because of poor or absent visibility of the posterior LC/scleral boundaries.[26] On average, the en face sectoral visibility of the anterior LC in the post-TE volumes (after compensation) was 58.6% (inferonasal), 57.4% (nasal), 59.9% (superonasal), 81.0% (superotemporal), 73.2% (temporal), and 68.1% (inferotemporal). Note that for the purpose of this study, only a single ONH geometry per eye needs to be reconstructed (pre-TE or post-TE) because the second can be "morphed" from such segmented reconstruction using the 3D displacements derived from 3D tracking.

Table 1. Demographic and Clinical Characteristics of Included Study Subjects

				IOP (mmHg)			Axial Length (mm)			Time (in Days)		
Patient	**Gender**	**Age, yrs**	**Study Eye**	*V1*	*V2*	*Change*	*V1*	*V2*	*Change*	*V1–TE*	*TE–V2*	*V1–V2*
POAG1	F	78	Left	14	10	4	22.8	22.82	0.02	0	36	36
POAG2	F	77	Right	12	6	6	24.34	Unavailable	Unavailable	20	22	42
POAG3	F	78	Left	9	5	4	23.55	23.37	−0.18	21	23	44
POAG4	F	67	Left	36	12	24	23.14	22.86	−0.28	0	38	38
POAG5	F	47	Left	35	23	12	24.33	24.29	−0.04	0	21	21
POAG6	F	50	Right	24	11	13	24.39	24.29	−0.1	0	50	50
POAG7	M	69	Right	23	17	6	23.14	23.16	0.02	6	49	55
POAG8	M	77	Left	49	24	25	24.37	24.22	−0.15	0	47	47
N1	M	38	Left	15	-	-	27.22	-	-	-	-	-
N2	M	37	Left	14	-	-	26.56	-	-	-	-	-
N3	F	25	Left	16	-	-	23.19	-	-	-	-	-

IOP = intraocular pressure; N = normal controls; POAG = primary open-angle glaucoma; TE = trabeculectomy; V1 = first visit (pre-TE); V2 = second visit (post-TE).
Note that IOP and axial length measurements were performed only once in the normal controls because OCT acquisitions were acquired twice consecutively in each patient.

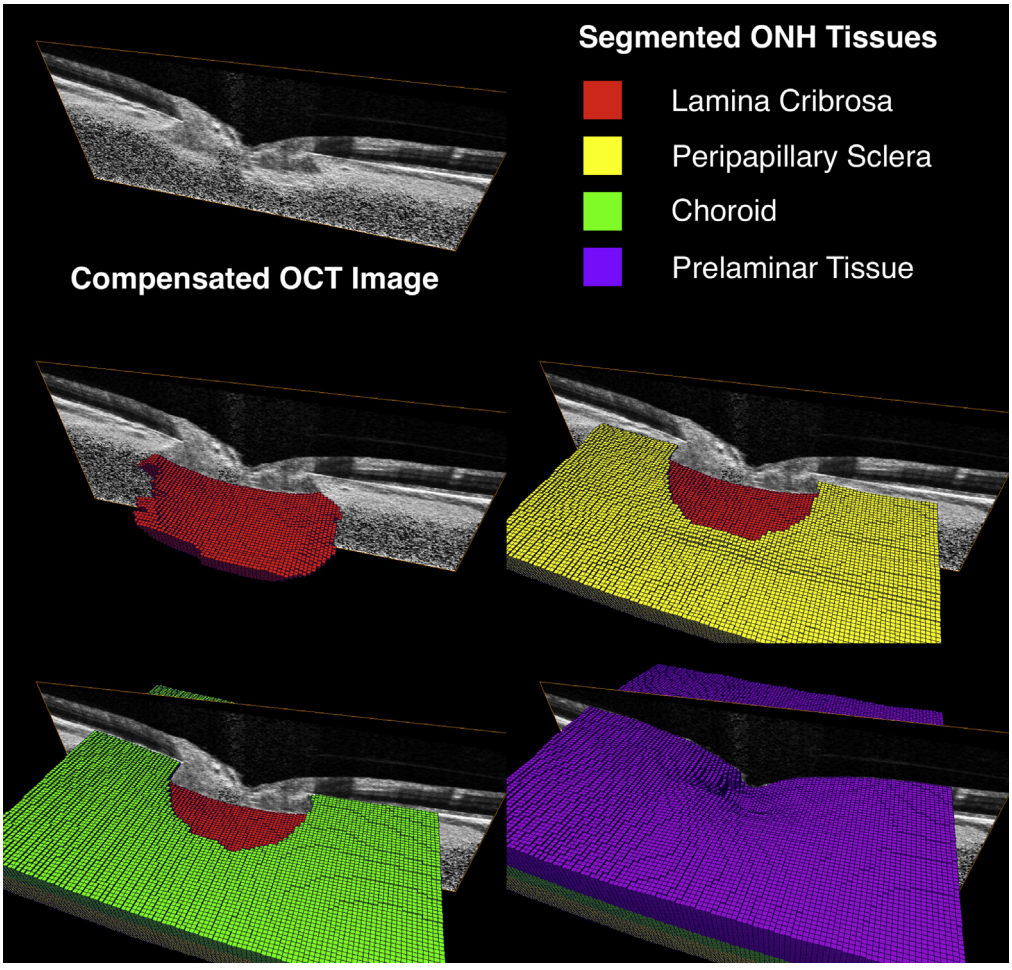

Figure 1. For each post-trabeculectomy (TE) optical coherence tomography (OCT) volume, the lamina cribrosa (LC) (red), peripapillary sclera (yellow), choroid (green), and prelaminar tissue (purple) were manually segmented. All segmented geometries were meshed using cubic elements. Note that the LC and peripapillary sclera were segmented only partially, that is, when the OCT signal for collagen was deemed visible. ONH = optic nerve head.

Biomechanical Mapping (Displacement and Strain)

Displacement and strain mapping were performed from the post-TE (lower IOP) volume to the pre-TE (higher IOP) volume for each subject's ONH. In this study, strain, or more accurately stated as "strain relief," is defined as the amount of local tissue deformation that has been relieved as the result of IOP lowering via TE. Specifically, tensile strain (or first principal strain) relief is defined as the local amount of tissue stretch that has been relieved after TE. Compressive strain (or third principal strain) relief is defined as the local amount of tissue compression that has been relieved after TE. The effective strain relief is a single index that conveniently summarizes the 3D state of strain relief and that combines both compressive and tensile effects.[28] In other words, the higher the compressive or tensile relief, the higher the effective strain relief.

When reporting displacements, the following convention was adopted: Positive displacements indicate anterior movement (with respect to the plane of Bruch's membrane) after IOP lowering, and negative displacements indicate posterior movement.

3-Dimensional Displacements. We have previously proposed and verified (but not validated) an OCT-based 3D tracking algorithm that can extract ONH displacements and strains. Here, we use this 3D tracking algorithm to extract ONH displacements/strains after IOP lowering by TE. Briefly, the tracking algorithm defines regions of interest (here: 51×51×21 voxels) in the post-TE OCT volume and then subjects them to mechanical transformations (rigid translation, rigid rotation, stretch/compression, and shear) until they best match their co-localized regions of interest in the pre-TE OCT volume.[33] To enhance the accuracy of each subject's IOP-induced displacement field, this later was (1) solved robustly during tracking using differential evolution (self-adapting scale factor $0.1 < F < 1$ and cross-over probability $0 < Cr < 1$)[34]; (2) processed for noise removal using spectral subtraction (signal-to-noise-ratio scaling factor $\alpha = 2$ and power spectrum parameter $a = 2$)[35,36]; (3) filtered from "bad vectors" (when x, y, and z displacements exceeded 3.5 times their corresponding median displacements in a surrounding local volume, i.e., 12.5% of the total OCT volume)[28]; and (4) smoothed (smoothing parameter $s = 0.3$; iteration number = 300; custom Matlab function "smoothn").[37] Control parameters for these operations were optimized to provide the smallest displacement errors for several test-case scenarios as performed in our previous study.[28] For all subjects, displacements were referenced with respect to the plane of Bruch's membrane.

3-Dimensional Strains. Once displacements were obtained, the tensile, compressive, and effective strain relief components were obtained and mapped through derivation of the displacement field.[28]

Additional Exclusion of Lamina Cribrosa Points from All Analyses

With tracking, it was possible for a displacement vector (originating from a visible portion of the LC in the post-TE volumes) to point to a region with "poor" OCT signal (in the pre-TE volumes) because signal information from neighboring voxels (with good signal) in the pre-TE volumes was used in the region of interest−matching process. This phenomenon, referred to as "anchoring," mostly affected the LC because its visibility varied between the pre- and post-TE volumes. By overlapping the segmented visible LC in the pre-TE volumes with the segmented (and deformed) visible LC in the post-TE volumes, we estimated that anchoring could occur on average for 13.76% of the LC (Supplemental Fig 1; available at www.aaojournal.org) or 0.98% of the entire ONH. To eliminate the anchoring phenomenon from our data, we excluded all LC points with displacement vectors that pointed to LC regions with poor signal in the pre-TE volumes from all our analyses. The excluded LC points were selected manually from the overlapping pre-TE and post-TE (deformed) geometries. These LC points then were removed from all post-TE ONH reconstructions.

3-Dimensional Tracking Validation

Normal control subjects recruited in this study provided validation for our methodology. Displacement and strain magnitudes reported in the normal controls should indicate the accuracy of our strain/displacement measurements because no IOP manipulations were performed in those patients.

To provide an additional degree of validation for this work, each obtained displacement field was applied to the post-TE (lower-IOP) segmented geometry. The resulting "deformed" geometry was manually superimposed with the pre-TE (higher-IOP) OCT volume to ensure that the key ONH tissue boundaries (anterior LC, choroidal-scleral interface, Bruch's membrane, inner limiting membrane) aligned with those observed in the pre-TE OCT images. This process was performed manually by 2 expert delineators (M.J.A.G., N.G.S.).

Statistical Analysis

To study the effects of TE on local ONH deformations, the ONHs of all glaucoma subjects were divided into 8 sectors of 45 degrees with respect to the center of the Bruch's membrane opening ellipse. The 50th (median) and 95th percentile displacements and strains (effective, tensile, and compressive) for the temporal, superotemporal, superior, superonasal, nasal, inferonasal, inferior, and inferotemporal sectors of the subjects were extracted and statistically analyzed using generalized estimating equations in R 3.0.2 (R Foundation, Vienna, Austria).[38] Generalized estimating equations allow the model fit to account for intra-sector associations within the same subject. Tissue type and sector location were used as categoric values for this analysis. Strain and displacement differences across sectors and across tissues (using median and 95th percentile values for each sector and each tissue) were investigated.

To understand the potential associations between LC strain relief and retinal sensitivity, the ONHs of the patients with glaucoma were divided into 6 sectors according to the regionalization scheme of Garway-Heath et al.[39] Visual field tests (24-2 program, Humphrey Field Analyzer, Carl Zeiss Meditec, Dublin, CA) undertaken at the time of listing for TE surgery were analyzed. The 52 retinal sensitivity data points extracted from these visual field maps were divided into 6 areas (according to the scheme of Garway-Heath et al[39]), and each point was unlogged before computing the median for respective areas. The median was then logged and reported in decibels. Median strains (effective, tensile, and compressive) for the temporal, superotemporal, superonasal, nasal, inferonasal, and inferotemporal sectors of the subjects were extracted. Considering that the 6 sectors from the ONH of a patient would be expected to have some degree of intercorrelation, generalized estimating equation models were used to analyze the associations between LC median strain and median retinal sensitivity, while accounting for the correlation. Finally, linear regressions were used to understand the potential associations between the magnitude of IOP decrease (from TE) and tissue strains/displacements (1 median value for each tissue and each eye).

Results

For all eyes, the maps of IOP-induced displacements are presented in Figure 2, and the maps of tensile, compressive, and effective

strain relief are shown in Figure 3. Effective strain relief medians (for each tissue and each subject) are presented in Table 2.

Validation (Normal Controls vs. Glaucoma Subjects)

In the normal control subjects, mean displacements (N1: 0.76±1.16 μm; N2: −9.7e-03±1.13 μm; N3: 0.15±2.80 μm) and effective strains (N1: 1.13%±0.34%; N2: 0.74%±0.20%; N3: 1.33%±0.46%) were small (Figs 2 and 3) and always lower than those in the subjects with glaucoma (mean displacement: −2.22±11.18 μm; mean effective strain: 8.6%±4.3%). These results also were true when considering tensile and compressive strains (Fig 3).

For each ONH, pre-TE tissue boundaries (derived from 3D tracking) aligned well with the pre-TE OCT images. An example is shown in Figure 4, where the LC of subject POAG6 was first segmented from the post-TE volume (Fig 4A). The pre-TE LC shape was then derived from 3D tracking (Fig 4B) and was shown to align well with the pre-TE OCT images (Fig 4B; alignment is shown for 2 B-scans).

Displacement and Strain Relief (Subjects with Glaucoma)

After TE, IOP in the subjects with glaucoma decreased from 25.3±13.9 mmHg to 13.5±7.19 mmHg (IOP decrease: 11.8±8.6 mmHg) (Table 1). In response to IOP lowering in the glaucoma eyes, the LC displaced (median) posteriorly in 3 eyes (POAG3: −29.37 μm; POAG4: −39.27 μm; POAG8: −34.57 μm), displaced anteriorly in 1 eye (POAG6: 100.5 μm), and was relatively stable (<2 times the height of a pixel) in 4 other eyes (POAG1: 1.09 μm; POAG2: −1.33 μm; POAG5: −5.69 μm; POAG7: −1.79 μm) (Fig 2).

We found no linear associations between the magnitude of IOP decrease and the LC displacements ($P = 0.61$) or LC effective strains ($P = 0.59$) (Fig 5). Note that these results were consistent for all tissues ($P > 0.05$), except for the choroid for which a weak association between IOP decrease and displacement was observed ($P = 0.05$).

On average, we found the largest anterior displacements (with respect to the plane of BMO) in the prelaminar tissues (red color in Fig 2), and such displacements (50th percentile: 5.40 μm; 95th percentile: 29.73 μm) were significantly different from all other tissues ($P < 0.01$). After IOP lowering, the prelaminar tissues thickened by 1.7% (50th percentile).

Higher compressive strain relief was observed in the sclera (median: 9.29%) and the choroid (8.45%), and this was significantly higher than that of the prelaminar tissue (6.69%; $P < 0.01$) and LC (6.75%; $P < 0.05$). Higher tensile strain relief was observed in the LC (9.57%), and this was significantly higher than that of the prelaminar tissue (6.62%; $P < 0.05$) and the choroid (5.78%; $P < 0.01$). For any given tissue, we found no differences in strain relief (all components) or displacement across sectors ($P > 0.05$).

Strain Relief versus Retinal Sensitivity (Subjects with Glaucoma)

By using sectorial strain data (median) and their corresponding sectorial retinal sensitivity values (median) for all 8 glaucoma ONHs (6 median values per ONH; 1 for each of 6 sectors), we found an association between raw retinal sensitivity (in decibels from visual field testing) and LC effective strain relief ($P < 0.001$) (Fig 6).

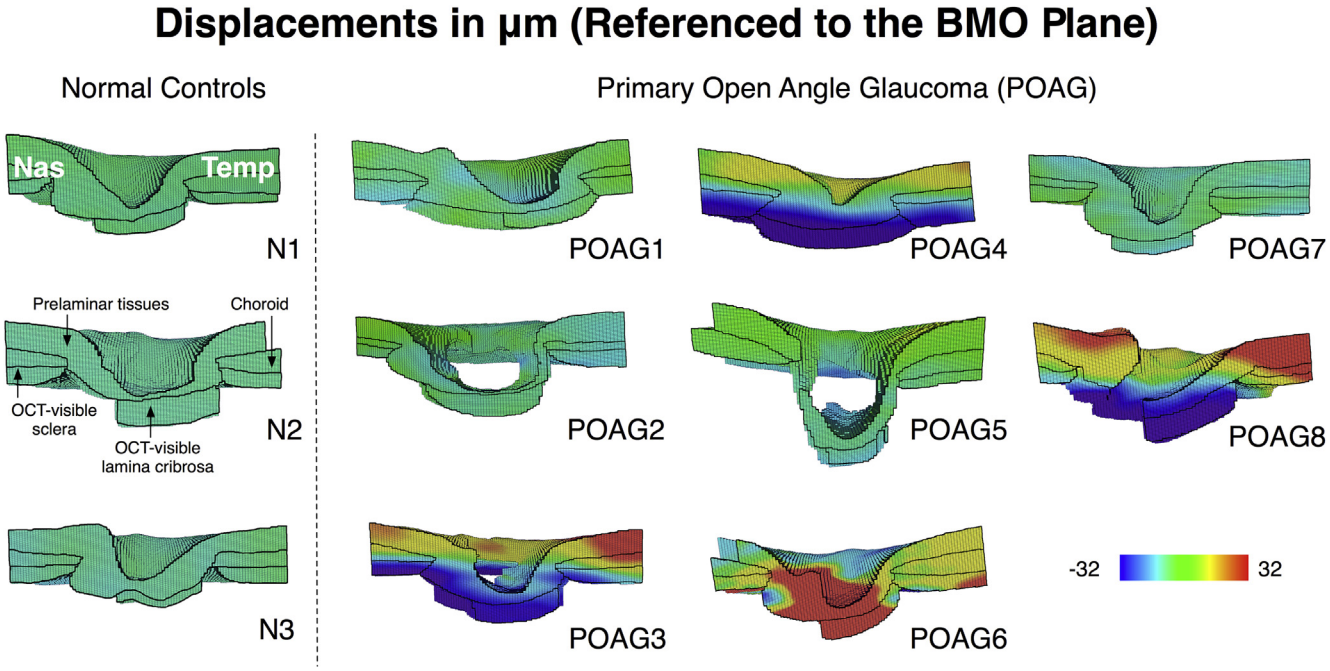

Figure 2. Color maps of intraocular pressure (IOP)-induced displacement (referenced to the plane of Bruch's membrane opening [BMO]) superimposed on clipped optic nerve head (ONH) geometries. Note that ONH tissues in the normal controls exhibited little displacement (mostly green). After IOP lowering by trabeculectomy (TE), the lamina cribrosa (LC) exhibited posterior movement in 3 subjects (blue color in primary open-angle glaucoma [POAG]3, POAG4, and POAG8), exhibited anterior movement in 1 subject (red color POAG6), and was relatively stable in the remaining 4 subjects with glaucoma (POAG1, POAG2, POAG5, and POAG7). Note that all left eyes were flipped to a right-eye configuration. N = normal; Nas = nasal; OCT = optical coherence tomography; POAG = primary open-angle glaucoma; Temp = temporal.

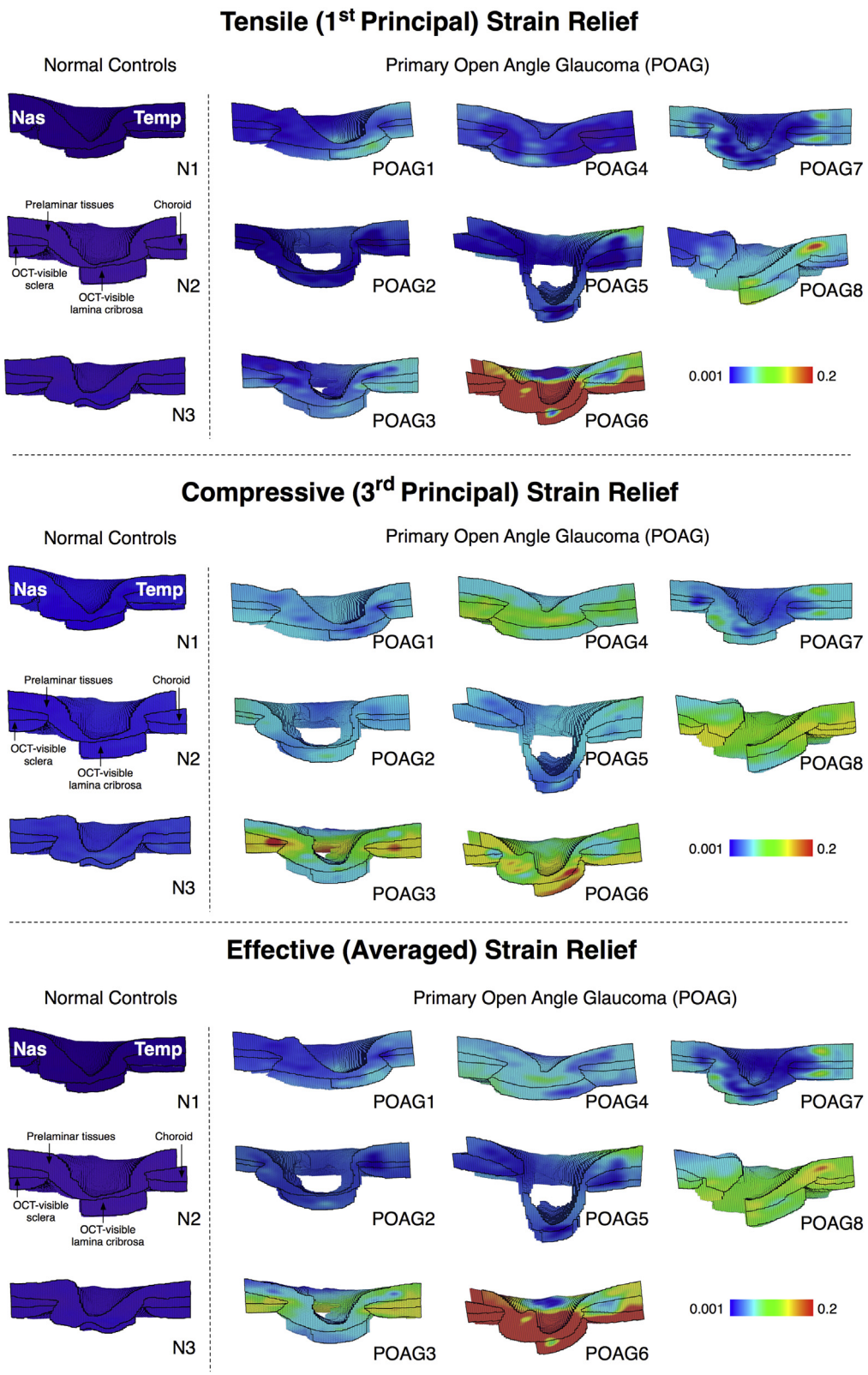

Figure 3. Color maps of tensile (first principal), compressive (third principal), and effective (averaged) strain relief superimposed on clipped ONH geometries. Note that ONH tissues in the normal controls exhibited little strain (mostly blue in all cases) as opposed to the glaucoma eyes. All left eyes were flipped to a right-eye configuration. N = normal; Nas = nasal; POAG = primary open-angle glaucoma; Temp = temporal.

Table 2. Median Effective Strain Relief for All Glaucoma and Normal Control Subjects

Patient	Median Effective Strain			
	Prelamina	*Choroid*	*Sclera*	*Lamina Cribrosa*
POAG1	0.0514	0.0518	0.0624	0.0656
POAG2	0.0559	0.0589	0.0563	0.0504
POAG3	0.0876	0.1290	0.1384	0.0625
POAG4	0.0738	0.0919	0.1001	0.0829
POAG5	0.0631	0.0581	0.0580	0.0513
POAG6	0.1577	0.1255	0.1945	0.3182
POAG7	0.0501	0.0425	0.0526	0.0787
POAG8	0.1168	0.1274	0.1264	0.1131
N1	0.0114	0.0117	0.0116	0.0094
N2	0.0076	0.0066	0.0069	0.0058
N3	0.0133	0.0133	0.0155	0.0170

N = normal controls; POAG = primary open-angle glaucoma.

Discussion

In this study, we have used an OCT-based 3D tracking technology[28] to map in vivo displacements/strains of ONH tissues after IOP lowering by TE. To the best of our knowledge, this is a novel and unique study to quantitatively map local 3D strains of the ONH in vivo and compare such measurements with measures of vision loss in a glaucoma population.

In this study, we demonstrated that IOP-induced 3D displacements and strains can be measured in vivo. Our technique was validated using manual segmentation and normal controls in whom IOP was unaltered. Furthermore, we found that performing TE was biomechanically beneficial for all patients with glaucoma in the sense that it relieved displacements and strains within all tissues. Specifically, when considering all patients with glaucoma, we found that the LC exhibited the highest tensile strain relief, the sclera and choroid exhibited the highest compressive strain relief, and the prelaminar tissue exhibited the highest anterior displacements. On average, the effective strain relief due to TE (8.6%) was higher than that measured in the normal controls (1.07%), indicating that IOP alone may be responsible for such deformations.

We found no associations between the magnitude of IOP decrease and that of LC strain relief (Fig 5) in the patients examined in this study. In other words, the largest IOP decrease (via TE) did not always provide the highest strain relief in the LC. Such a finding could have important clinical implications. First, it suggests that strong biomechanical variability may exist across eyes. Although some subjects may have "rigid" ONHs insensitive to IOP changes, others may exhibit weaker ONH biomechanical properties and thus larger deformations. For instance, age and race have been found to significantly influence ONH biomechanics.[9,40,41] Second, TE surgery often yields different outcomes. In some cases, visual field progression and ONH structural damage can continue to develop even if a stable IOP has been reached.[42] It may be possible that eyes that continue to progress are those that did not exhibit sufficient strain relief. Our aim is to test such a hypothesis in the near future, because it could considerably improve our understanding of glaucoma progression.

Of note, after IOP lowering, we observed that the LC displaced posteriorly in 3 eyes (mean: −34.3 μm), displaced anteriorly in 1 eye (98.9 μm), and was relatively stable in 4 other eyes (−1.89 μm). Recent OCT studies in subjects with glaucoma all have reported mean anterior LC displacements after TE,[20,21,25,43] and only 1 specific study (in agreement with ours) reported both posterior and anterior LC displacements in glaucomatous eyes (13.9% of subjects underwent glaucoma filtration surgery, 90% of which were TE) that were followed longitudinally for 2 years.[23] Our LC displacement data further reinforce the notion of biomechanical variability and are in agreement with model predictions performed by Sigal et al.[44] In such models, the LC was predicted to displace posteriorly, anteriorly, or not at all after a change in IOP. For instance, posterior LC displacement after TE, a counterintuitive concept, could be explained by a reduction in scleral canal size that could in turn lead to posterior buckling of the LC. Note also that we have reviewed our clinical observations, but we were unable to identify a reason for why only a single eye would exhibit anterior LC displacement in our study group. In particular, there was no detectable relationship with age, IOP at presentation, IOP at listing, number and type of IOP-lowering medications before listing, refraction, axial length, or associated systemic pathology. Lamina cribrosa displacement likely is to be influenced by key biomechanical factors, such as scleral/LC shape,[45] stiffness/thickness, and protein-fiber microarchitecture.[6] Understanding the links between these factors and LC deformations may prove critical for our understanding of glaucoma pathogenesis. Unfortunately, no techniques yet exist to measure ONH stiffness and protein-fiber microarchitecture in vivo.

In this study, we found an association between retinal sensitivity and LC effective strain relief, suggesting a potential link between local LC deformations and visual field damage. Such results may have important clinical implications. The IOP-induced LC strains have long been suspected to play significant roles in glaucoma pathogenesis, but no studies have been able to provide such measurements in vivo. Although speculations still exist, IOP-induced LC strains have the potential to (1) disrupt axoplasmic flow; (2) alter microcapillary blood flow; (3) increase RGC apoptosis; and (4) activate astrocytes, glial, and LC cells.[46] Accordingly, it may seem logical that a direct spatial correlation between LC deformations and visual field loss should exist. It is important to keep in mind that our data do not imply a causal relationship between strain and visual field loss. If such a correlation were to exist, it would need to be established in a prospective study with repeated ONH strain mapping and a much larger glaucoma cohort.

For any given tissue, we did not observe significant regional variations in strain relief. Fazio et al[47] observed higher IOP-induced strains in the inferotemporal region of the peripapillary sclera and suggested that such strains could be linked to glaucoma damage. Only a single study by Sigal

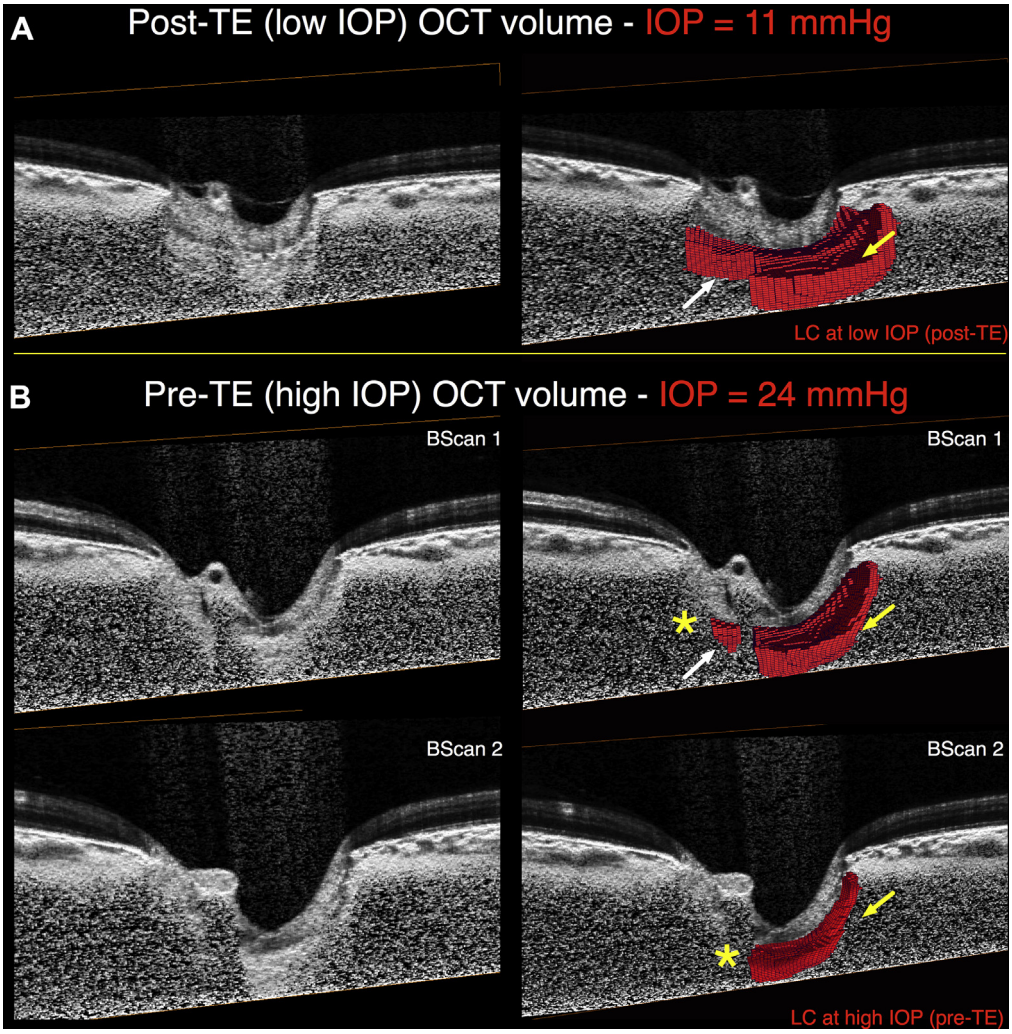

Figure 4. Manual validation of our 3-dimensional (3D) tracking technique shown for the lamina cribrosa (LC) of subject primary open-angle glaucoma (POAG)6. **A**, The LC was manually segmented from the post-trabeculectomy (TE) (low intraocular pressure [IOP]) optical coherence tomography (OCT) images. **B**, The pre-TE (high IOP) LC shape was then obtained from 3D tracking and was shown to align well with the pre-TE OCT images (as shown from 2 B-scans with and without superimposition of the pre-TE LC geometry). The *yellow arrow* indicates a region of high strain relief after TE, and the *white arrow* indicates a region of relatively lower strain relief. The *yellow asterisks* indicate poor LC visibility when segmentation and 3D tracking were not performed.

et al[10] has been able to map IOP-induced LC strains in ex vivo human eyes, but it did not report regional variations.[10] Strain responses likely are to be highly patient-specific. For instance, in subject POAG3, higher strain relief was observed in the temporal region (yellow arrow in Fig 4) than in the nasal region, but such a trend was not observed across all eyes. More subjects likely are needed to establish whether IOP-induced strain in the ONH tissues exhibit significant regional variability in vivo.

Study Limitations

Several limitations in this study warrant further discussion. First, the OCT acquisitions could not always be performed immediately before and after TE, and therefore the resulting ONH deformations cannot be strictly considered as those resulting from acute IOP changes. It is plausible that connective tissue growth/remodeling may have occurred within 8 weeks (the maximum time between 2 OCT acquisitions) after IOP lowering. Although no data are yet available to support such hypothesis in humans, it should be noted that ONH connective tissue remodeling (LC thickening) has been observed rapidly (<8 weeks) in monkeys subjected to chronic IOP elevations.[48] We are currently mapping ONH strains in a longitudinal study in subjects with glaucoma, which should allow us to distinguish acute from growth/remodeling deformations and their potential contributions to visual field loss.

Second, full-thickness segmentation of the sclera and LC could not be achieved because of limited tissue visibility in OCT. We have recently reported that in the best cases, the posterior LC was visible in only 21% of subjects, even after using enhancement techniques such as AC.[26] This directly implies that the performance of current OCT technology is

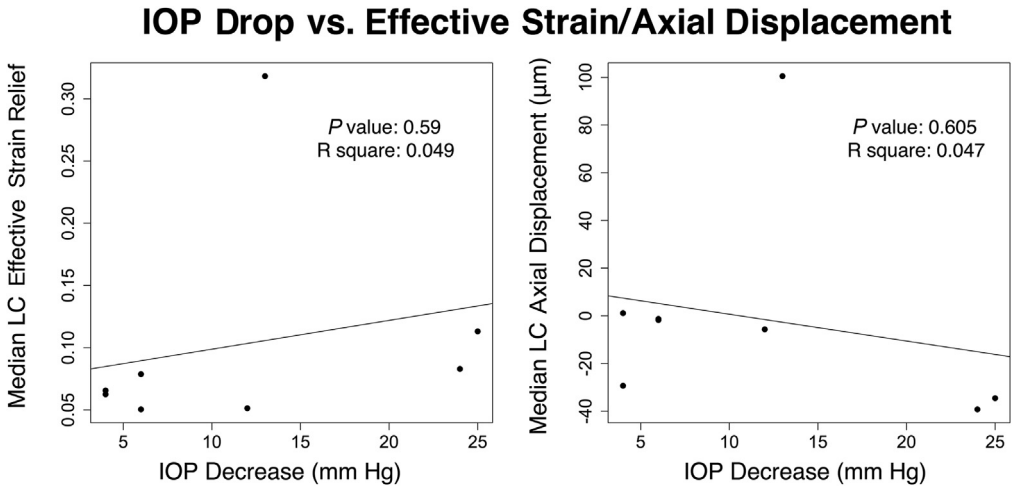

Figure 5. For each subject with glaucoma, the median effective strain relief and median axial displacement in the lamina cribrosa (LC) were obtained and plotted against the intraocular pressure (IOP) decrease after trabeculectomy (TE). When a linear model was fit to these data, a bad fit was obtained ($R^2 < 0.1$), suggesting no linear relationship between IOP decrease and strain/displacement for the subjects of this study.

not yet sufficient to test whether strains in the posterior LC or retrolamina could play an important role in glaucoma pathogenesis.

Third, the effective strain in the normal controls, in whom IOP was not altered, was found to be non zero and averaged 1.07% across all 3 subjects. The existence of strain in these subjects could be due to (1) OCT registration errors; (2) preprocessing and postprocessing errors; (3) speckle noise; or (4) potential IOP fluctuations across scans arising from ocular pulsations. This result implies limitations if one were to investigate the impact of IOP-induced strains of 1% or less in vivo. It is currently unknown whether LC cells and astrocytes would chemically respond to such small strain magnitudes because most studies that demonstrated the presence of mechanotransduction in ONH cells in vitro have considered only larger strains (15%,[49] 3%, and 12%[50]). To improve strain accuracy, it is worth mentioning that our proposed 3D tracking techniques could integrate seamlessly with advanced imaging modalities such as adaptive optics[51] or micro-OCT.[52] Nevertheless, we think our current strain accuracy should be sufficient to test biomechanical hypotheses as demonstrated in this article through a positive association between strain and visual field loss.

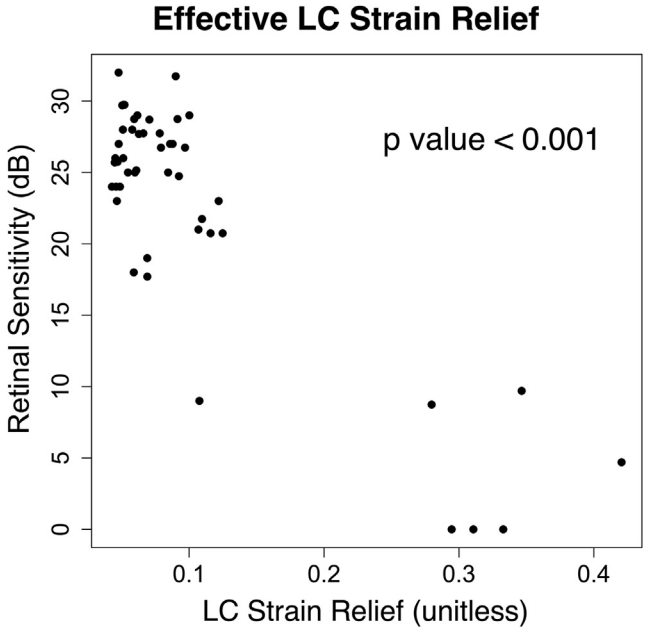

Figure 6. Associations between median retinal sensitivity and median lamina cribrosa (LC) strain relief (effective). Median LC strain relief was calculated for each sector (according to the regionalization scheme of Garway-Heath et al[39]) and for each patient, and then plotted against corresponding median retinal sensitivity. Note that the data are shown for all 8 subjects. dB = decibels.

Fourth, because of the proposed experimental design (IOP lowering via TE), we were unable to perform repeatability testing. In other words, IOP lowering could not be achieved twice under the exact same conditions in the same subject. Repeatability measurements will be able to be performed in future studies using ophthalmodynamometry. In addition, we were unable to compare our strain estimates because no quantitative 3D strain mapping technology has yet been proposed for the ONH in vivo.

We present here novel engineering tools that can map 3D local deformations of the ONH in vivo for the first time. We demonstrate that ONH displacements and strains are detectable in vivo and that TE can relieve strains in the ONH tissues. Our data also suggest a wide patient-to-patient variability in ONH biomechanical properties. We further demonstrated associations between LC strain relief and retinal sensitivity. Strain relief in the LC may be one explanation as to why glaucomatous progression is slowed after TE.

References

1. Sommer A, Tielsch JM, Katz J, et al. Relationship between intraocular-pressure and primary open angle glaucoma among

white and black Americans. The Baltimore Eye Survey. Arch Ophthalmol 1991;109:1090–5.
2. Leske MC, Wu SY, Hennis A, et al. Risk factors for incident open-angle glaucoma. Ophthalmology 2008;115:85–93.
3. Quigley HA. Glaucoma: macrocosm to microcosm: the Friedenwald lecture. Invest Ophthalmol Vis Sci 2005;46:2663–70.
4. Leske MC. Open-angle glaucoma: an epidemiologic overview. Ophthalmic Epidemiol 2007;14:166–72.
5. Girard MJ, Suh JK, Bottlang M, et al. Biomechanical changes in the sclera of monkey eyes exposed to chronic IOP elevations. Invest Ophthalmol Vis Sci 2011;52:5656–69.
6. Zhang L, Albon J, Jones H, et al. Collagen microstructural factors influencing optic nerve head biomechanics. Invest Ophthalmol Vis Sci 2015;56:2031–42.
7. Sigal IA, Ethier CR. Biomechanics of the optic nerve head. Exp Eye Res 2009;88:799–807.
8. Campbell IC, Coudrillier B, Ross Ethier C. Biomechanics of the posterior eye: a critical role in health and disease. J Biomech Eng 2014;136:021005.
9. Coudrillier B, Tian J, Alexander S, et al. Biomechanics of the human posterior sclera: age- and glaucoma-related changes measured using inflation testing. Invest Ophthalmol Vis Sci 2012;53:1714–28.
10. Sigal IA, Grimm JL, Jan NJ, et al. Eye-specific IOP-induced displacements and deformations of human lamina cribrosa. Invest Ophthalmol Vis Sci 2014;55:1–15.
11. Fazio MA, Grytz R, Morris JS, et al. Human scleral structural stiffness increases more rapidly with age in donors of African descent compared to donors of European descent. Invest Ophthalmol Vis Sci 2014;55:7189–98.
12. Cruz Perez B, Tang J, Morris HJ, et al. Biaxial mechanical testing of posterior sclera using high-resolution ultrasound speckle tracking for strain measurements. J Biomech 2014;47:1151–6.
13. Sigal IA, Flanagan JG, Ethier CR. Factors influencing optic nerve head biomechanics. Invest Ophthalmol Vis Sci 2005;46:4189–99.
14. Girard MJ, Downs JC, Burgoyne CF, Suh JK. Peripapillary and posterior scleral mechanics—part I: development of an anisotropic hyperelastic constitutive model. J Biomech Eng 2009;131:051011.
15. Grytz R, Meschke G, Jonas JB. The collagen fibril architecture in the lamina cribrosa and peripapillary sclera predicted by a computational remodeling approach. Biomech Model Mechanobiol 2011;10:371–82.
16. Ayyalasomayajula A, Park RI, Simon BR, Vande Geest JP. A porohyperelastic finite element model of the eye: the influence of stiffness and permeability on intraocular pressure and optic nerve head biomechanics. Comput Methods Biomech Biomed Engin 2015;1–12.
17. Girard MJ, Dupps WJ, Baskaran M, et al. Translating ocular biomechanics into clinical practice: current state and future prospects. Curr Eye Res 2015;40:1–18.
18. Agoumi Y, Sharpe GP, Hutchison DM, et al. Laminar and prelaminar tissue displacement during intraocular pressure elevation in glaucoma patients and healthy controls. Ophthalmology 2011;118:52–9.
19. Strouthidis NG, Fortune B, Yang H, et al. Effect of acute intraocular pressure elevation on the monkey optic nerve head as detected by spectral domain optical coherence tomography. Invest Ophthalmol Vis Sci 52:9431−9437.
20. Lee EJ, Kim TW, Weinreb RN. Reversal of lamina cribrosa displacement and thickness after trabeculectomy in glaucoma. Ophthalmology 2012;119:1359–66.
21. Reis AS, O'Leary N, Stanfield MJ, et al. Laminar displacement and prelaminar tissue thickness change after glaucoma surgery imaged with optical coherence tomography. Invest Ophthalmol Vis Sci 2012;53:5819–26.
22. Strouthidis NG, Fortune B, Yang H, et al. Longitudinal change detected by spectral domain optical coherence tomography in the optic nerve head and peripapillary retina in experimental glaucoma. Invest Ophthalmol Vis Sci 2012;52:1206–19.
23. Wu Z, Xu G, Weinreb RN, et al. Optic nerve head deformation in glaucoma: a prospective analysis of optic nerve head surface and lamina cribrosa surface displacement. Ophthalmology 2015;122:1317–29.
24. Lee EJ, Kim TW, Weinreb RN, Kim H. Reversal of lamina cribrosa displacement after intraocular pressure reduction in open-angle glaucoma. Ophthalmology 2013;120:553–9.
25. Park HY, Shin HY, Jung KI, Park CK. Changes in the lamina and prelamina after intraocular pressure reduction in patients with primary open-angle glaucoma and acute primary angle-closure. Invest Ophthalmol Vis Sci 2014;55:233–9.
26. Girard MJ, Tun TA, Husain R, et al. Lamina cribrosa visibility using optical coherence tomography: comparison of devices and effects of image enhancement techniques. Invest Ophthalmol Vis Sci 2015;56:865–74.
27. Mari JM, Strouthidis NG, Park SC, Girard MJ. Enhancement of lamina cribrosa visibility in optical coherence tomography images using adaptive compensation. Invest Ophthalmol Vis Sci 2013;54:2238–47.
28. Girard MJ, Strouthidis NG, Desjardins A, et al. In vivo optic nerve head biomechanics: performance testing of a three-dimensional tracking algorithm. J R Soc Interface 2013;10:20130459.
29. National Collaborating Centre for Acute Care. National Institute for Health and Clinical Excellence: Guidance. Glaucoma: Diagnosis and Management of Chronic Open Angle Glaucoma and Ocular Hypertension. London: National Collaborating Centre for Acute Care (UK); 2009.
30. Jayaram H, Strouthidis NG, Kamal DS. Trabeculectomy for normal tension glaucoma: outcomes using the Moorfields Safer Surgery technique. Br J Ophthalmol 2016;100:332–8.
31. Girard MJ, Strouthidis NG, Ethier CR, Mari JM. Shadow removal and contrast enhancement in optical coherence tomography images of the human optic nerve head. Invest Ophthalmol Vis Sci 2011;52:7738–48.
32. Gupta P, Sidhartha E, Girard MJ, et al. A simplified method to measure choroidal thickness using adaptive compensation in enhanced depth imaging optical coherence tomography. PLoS One 2014;9:e96661.
33. Price KV, Storn RM, Lampinen JA. Differential Evolution. A Practical Approach to Global Optimization. Berlin, Germany: Springer; 2005.
34. Brest J, Greiner S, Boskovic B, et al. Self-adapting control parameters in differential evolution: a comparative study on numerical benchmark problems. Trans Evol Comp 2006;10:646–7.
35. Lu Y, Loizou PC. A geometric approach to spectral subtraction. Speech commun 2008;50:453–66.
36. Vaseghi SV. Spectral Amplitude Estimations. In: Advanced Digital Signal Processing and Noise Reduction. 3rd ed. Hoboken, NJ: Wiley; 2006:480.
37. Garcia D. Robust smoothing of gridded data in one and higher dimensions with missing values. Comput Stat Data Anal 2010;54:1167–78.
38. Hojsgaard S, Halekoh U, Yan J. The R package geepack for generalized estimating equations. J Stat Softw 2006;15:1–11.
39. Garway-Heath DF, Poinoosawmy D, Fitzke FW, Hitchings RA. Mapping the visual field to the optic disc in

normal tension glaucoma eyes. Ophthalmology 2000;107:1809–15.
40. Girard MJ, Suh JK, Bottlang M, et al. Scleral biomechanics in the aging monkey eye. Invest Ophthalmol Vis Sci 2009;50:5226–37.
41. Grytz R, Fazio MA, Libertiaux V, et al. Age- and race-related differences in human scleral material properties. Invest Ophthalmol Vis Sci 2014;55:8163–72.
42. Landers J, Martin K, Sarkies N, et al. A twenty-year follow-up study of trabeculectomy: risk factors and outcomes. Ophthalmology 2012;119:694–702.
43. Lee EJ, Kim TW, Weinreb RN. Improved reproducibility in measuring the laminar thickness on enhanced depth imaging SD-OCT images using maximum intensity projection. Invest Ophthalmol Vis Sci 2012;53:7576–82.
44. Sigal IA, Yang H, Roberts MD, et al. IOP-induced lamina cribrosa deformation and scleral canal expansion: independent or related? Invest Ophthalmol Vis Sci 2011;52:9023–32.
45. Thakku SG, Tham YC, Baskaran M, et al. A global shape index to characterize anterior lamina cribrosa morphology and its determinants in healthy Indian eyes. Invest Ophthalmol Vis Sci 2015;56:3604–14.
46. Strouthidis NG, Girard MJA. Altering the way the optic nerve head responds to intraocular pressure—a potential approach to glaucoma therapy. Curr Opin Pharmacol 2013;13:83–9.
47. Fazio MA, Grytz R, Bruno L, et al. Regional variations in mechanical strain in the posterior human sclera. Invest Ophthalmol Vis Sci 2012;53:5326–33.
48. Yang H, Downs JC, Girkin C, et al. 3-D histomorphometry of the normal and early glaucomatous monkey optic nerve head: lamina cribrosa and peripapillary scleral position and thickness. Invest Ophthalmol Vis Sci 2007;48:4597–607.
49. Kirwan RP, Fenerty CH, Crean J, et al. Influence of cyclical mechanical strain on extracellular matrix gene expression in human lamina cribrosa cells in vitro. Mol Vis 2005;11:798–810.
50. Rogers RS, Dharsee M, Ackloo S, et al. Proteomics analyses of human optic nerve head astrocytes following biomechanical strain. Mol Cell Proteomics 2012;11. M111.012302.
51. Kim TW, Kagemann L, Girard MJ, et al. Imaging of the lamina cribrosa in glaucoma: perspectives of pathogenesis and clinical applications. Curr Eye Res 2013;38:903–9.
52. Liu L, Gardecki JA, Nadkarni SK, et al. Imaging the subcellular structure of human coronary atherosclerosis using micro-optical coherence tomography. Nat Med 2011;17:1010–4.

Footnotes and Financial Disclosures

Originally received: August 18, 2015.
Final revision: January 29, 2016.
Accepted: February 3, 2016.
Available online: ■■■. Manuscript no. 2015-1426.

[1] Ophthalmic Engineering & Innovation Laboratory, Department of Biomedical Engineering, National University of Singapore, Singapore.

[2] Singapore Eye Research Institute, Singapore National Eye Centre, Singapore.

[3] NIHR Biomedical Research Centre at Moorfields Eye Hospital NHS Foundation Trust and UCL Institute of Ophthalmology, London, United Kingdom.

[4] Université de la Polynésie française, Tahiti, French Polynesia.

[5] Discipline of Clinical Ophthalmology and Eye Health, University of Sydney, Sydney, NSW, Australia.

Presented in part at: the Association for Research in Vision and Ophthalmology annual meeting, May 5–9, 2013, Seattle, Washington.

Financial Disclosure(s):

The author(s) have made the following disclosure(s): M.J.A.G.: Consultant – Singapore Eye Research Institute; Support – Ministry of Education, Academic Research Funds, Tier 1 (R-397-000-140-133); and an NUS Young Investigator Award (NUSYIA_FY13_P03, R-397-000-174-133).

N.G.S.: Lecture fees/honoraria – Heidelberg, Alcon, Allergan, and Novartis.

N.G.S.: Received a proportion of his financial support from the UK Department of Health through the award made by the National Institute for Health Research to Moorfields Eye Hospital NHS Foundation Trust and UCL Institute of Ophthalmology for a Biomedical Research Centre for Ophthalmology. The views expressed in this publication are those of the authors and not necessarily those of the UK Department of Health.

Author Contributions:

Conception and design: Girard, Strouthidis

Data collection: Girard, Beotra, Chin, Sandhu, Clemo, Nikita, Kamal, Papadopoulos, Mari, Aung, Strouthidis

Analysis and interpretation: Girard, Beotra, Chin, Sandhu, Clemo, Nikita, Kamal, Papadopoulos, Mari, Aung, Strouthidis

Obtained funding: Girard, Strouthidis

Overall responsibility: Girard, Strouthidis

Abbreviations and Acronyms:

AC = adaptive compensation; **IOP** = intraocular pressure; **LC** = lamina cribrosa; **OCT** = optical coherence tomography; **ONH** = optic nerve head; **POAG** = primary open-angle glaucoma; **TE** = trabeculectomy; **3-D** = 3-dimensional.

Correspondence:

Michaël J.A. Girard, MSc, PhD, Ophthalmic Engineering & Innovation Laboratory, Department of Biomedical Engineering, National University of Singapore, 4 Engineering Drive 3, E4-04-08, 117583, Singapore. E-mail: mgirard@nus.edu.sg.